International Food Research Journal 31(4): 858 - 871 (August 2024)
Journal homepage: *http://www.ifrj.upm.edu.my*

Poly(lactic acid)/silver/benzyl dodecyl dimethylammonium modified montmorillonite nanocomposite with antifungal activity for food packaging application

[1]Lertkongyos, P., [1,2]*Songtipya, P., [1,2]Prodpran, T., [1,2]Pisuchpen, S. and [1,2]Songtipya, L.

[1]Food Packaging Technology Program, Faculty of Agro-Industry, Prince of Songkla University, Hat Yai, Songkhla, 90110, Thailand
[2]Center of Excellence in Bio-Based Materials and Packaging Innovation, Faculty of Agro-Industry, Prince of Songkla University, Hat Yai, Songkhla, 90110, Thailand

Article history

Received:
22 August 2023
Received in revised form:
6 May 2024
Accepted:
10 June 2024

Keywords

poly(lactic acid), nanocomposite, silver, montmorillonite, antifungal activity, food packaging, benzyl dodecyl dimethylammonium chloride

Abstract

Active biodegradable food packaging with antimicrobial properties is desirable for prolonging the shelf life of food products while minimising waste streams originating from the food supply chain. In the present work, a novel antifungal nanocomposite was prepared by a two-step melt-blending process using poly(lactic acid) (PLA) incorporated with 5 and 8 php of modified clay. The modified clay consisted of sodium montmorillonite (Na^+-Mt) modified with silver (Ag) and benzyl dodecyl dimethylammonium chloride (BDAC) at different Ag and BDAC ratios. X-ray diffraction spectra and photomicrographs revealed the distribution of Ag particles and modified Mt layers in the PLA matrix, resulting in an intercalated structure. The antifungal activity of the PLA-based nanocomposites was tested against some foodborne pathogenic fungi *Penicillium roqueforti* and *Fusarium moniliforme*. The tensile strength and elongation at break of the nanocomposites decreased, whereas Young's modulus increased compared with neat PLA. Incorporating 5 php of Ag20/BDAC80-Mt into the nanocomposite resulted in the highest impact strength. The water vapour permeability of the nanocomposite was comparable to that of neat PLA. Differential scanning calorimetry (DSC) showed a decrease in the T_g and T_{cc} of the nanocomposites, although the T_m did not change. For the PLA/Ag20/BDAC80-Mt-5 nanocomposite, the overall migration in distilled water, acetic acid (3%, w/v), and ethanol (10%, v/v) was below 10 mg/dm^2. Overall, the present work demonstrated the potential of the modified clay for developing antifungal active bionanocomposites for food packaging applications.

DOI
https://doi.org/10.47836/ifrj.31.4.05

Introduction

Microbial food spoilage affects the shelf life of packaged foods, resulting in food waste, economic losses, and health risks. Therefore, active polymeric food packaging has gained much attention for preserving food quality and safety, and extending shelf life. Active packaging can be produced by incorporating antimicrobial agents into polymers, and offers benefits over traditional food preservatives (Moeini *et al*., 2021).

Sustainable biodegradable polymers are of particular interest because they are environmentally friendly. Poly(lactic acid) (PLA) is an alternative to petroleum-based polymers due to its availability, high strength and modulus, processability, low energy requirements, biodegradability, and biocompatibility. However, PLA has some drawbacks, such as brittleness, low thermal stability, high permeation to moisture and oxygen, slow degradation, hydrophobicity, and lack of side groups, which limits it applications (Auras *et al*., 2004; Zhong *et al*., 2020).

Polymer nanocomposites exhibit advantages compared to the neat polymers and conventional composites. Polymer nanocomposites are produced using nanoparticles as fillers, requiring only a small amount to improve the properties of the polymer matrix. These improvements are generally associated with the high surface area and aspect ratio of nanoscale fillers (Dharini *et al*., 2022; Priyadarshi *et al*., 2022; Shi *et al*., 2023). Layered silicate,

*Corresponding author.
Email: ponusa.j@psu.ac.th

particularly montmorillonite (Mt), is one of the most attractive nanofillers. Nevertheless, to produce nonpolar polymeric nanocomposites, the clay's polarity should be altered to make it more organophilic. This can be attained using cationic surfactants (*e.g*., cationic quaternary ammonium ions), some of which display antimicrobial activity, both in free form and when immobilised on the Mt surface (Khalil, 2013; Mohapatra *et al*., 2023; Moustafa *et al*., 2023).

Benzyl dodecyl dimethylammonium chloride (BDAC), a broad-spectrum synthetic quaternary ammonium antimicrobial agent, is extensively used as a disinfectant in the food industry and healthcare products, such as hand sanitisers, intranasal products, and disinfectants (Khalil, 2013; Haubert *et al*., 2019; Zhao *et al*., 2024).

Silver (Ag) ions are powerful antimicrobial agents with a long history of use. Silver exhibits broad-spectrum antimicrobial activity, is safely used in minute concentrations, and possesses high thermal stability and low volatility. The development of Ag-loaded organo-Mt with strong antimicrobial activity has been reported (Zhang *et al*., 2018; Fernández Solarte *et al*., 2019; Hong *et al*., 2022). Most studies have focused on antibacterial activity, whereas studies on antifungal activity are limited. The most common foodborne pathogenic fungi belong to the genera *Penicillium*, *Aspergillus*, *Botrytis*, *Monilia*, *Endomyces*, *Eurotium*, *Cladosporium*, *Fusarium*, *Geotrichum*, *Rhizopus*, and *Wallemia* (Santagata *et al*., 2017; Valerio *et al*., 2018).

In the present work, we synthesised $AgNO_3$/BDAC-modified Mt (Ag/BDAC-Mt), and incorporated it into PLA. We investigated the nanocomposite's structure, mechanical, thermal, and water vapour barrier properties, overall migration, and antifungal activity against foodborne pathogenic and mycotoxigenic strains. The present work focused on *Penicillium roqueforti*, the main contaminant in bakery products and cheeses (Santagata *et al*., 2017; Moeini *et al*., 2020), and *Fusarium verticillioides* (formerly *F. moniliforme*), which occurs in maize, sorghum, rice, millet, and many other crops, and also causes the spoilage of citrus, asparagus, yams, bananas, and pineapples (Tola and Kebede, 2016; Kant *et al*., 2017). The intended benefit of Ag/BDAC-Mt is to enhance dispersion in the PLA matrix while conferring an antifungal effect for active food packaging.

Materials and methods

Materials

PLA (4032D, M_n = 88,500 g/mol, and M_w/M_n = 1.8) was purchased from NatureWorks Co., Ltd. (USA). The PLA had an L-to-D-lactide ratio of 28:1 according to the supplier. Polybond 3009 (HDPE-g-MA), a high-density polyethylene (HDPE) grafted with MA (1 wt.%) and having MFI = 5 dg/min was procured from Chemtura Corporation (USA). Na^+-Mt (Cloisite Na^+) was supplied by Southern Clay Products Inc. (USA), with a cation exchange capacity (CEC) of 92 meq/100 g according to the supplier. Benzyl dodecyl dimethylammonium chloride (BDAC, 99% purity, molecular weight 339.99 g/mol) was purchased from Sigma-Aldrich Inc. (USA), and the cationic surfactant used to modify Na^+-Mt. Silver nitrate ($AgNO_3$, 99.9% purity, molecular weight 169.87 g/mol) was purchased from Merck (USA). Ethanol (99%) was purchased from Lab Scan Analytical Science (Thailand). Acetic acid (99.7% purity) was procured from Loba Chemie (India). Nutrient broth, nutrient agar, potato dextrose broth (PDB), and potato dextrose agar (PDA) were purchased from Himedia Laboratories (India). Deionised water (Millipore) was used in all experiments. All chemicals were of analytical grade, and used as received.

Microorganisms

Penicillium roqueforti TISTR2011 and *Fusarium moniliforme* TISTR3175 were chosen based on their different growth rates, and obtained from the Thailand Institute of Scientific and Technological Research (TISTR).

Na^+-Mt modification

Ag-modified montmorillonite was prepared by reacting an $AgNO_3$ solution with Na^+-Mt, following the method of Ohashi *et al*. (2009) with modifications. Briefly, Na^+-Mt (10 g) was dispersed in 800 mL of deionised water, stirred at 70°C for 1 h, and sonicated for 10 min in a sonication bath. $AgNO_3$ was dissolved in 50 mL of deionised water. The mixture was then gradually added to the Na^+-Mt dispersion. The dispersion was further stirred for 24 h. The solid slurry was separated by centrifugation at 500 rpm for 5 min. Finally, the sediment was washed with deionised water, and vacuum-dried overnight at 70°C. The dried samples were ground using a mortar

and pestle until a homogenous powder was obtained. BDAC-Mt was prepared *via* a cation exchange reaction by adding a BDAC solution to the Na^+-Mt suspension, followed by washing with deionised water until it was free of residual halide ions (silver nitrate test). The preparation of Ag/BDAC-Mt was similar to that of BDAC-Mt, with Na^+-Mt replaced with BDAC-Mt. Ag/BDAC-Mt was washed with distilled water until no unbound ions remained. The Ag:BDAC ratios, as different percentages of the total CEC of Na^+-Mt, were 100:0, 20:80, 50:50, 80:20, and 100:0, and assigned sample codes Ag-Mt, Ag20/BDAC80-Mt, Ag50/BDAC50-Mt, Ag80/BDAC20-Mt, and BDAC-Mt, respectively.

Preparation of PLA nanocomposite

PLA pellets and modified Mt powder (Ag-Mt, BDAC-Mt, and Ag20/BDAC80-Mt) were dried overnight at 60°C under vacuum. PLA nanocomposites were prepared using a masterbatch approach. A twin-screw extruder (Prism TSE16TC) was used to compound the modified Mt and polymers at 175°C (Zone 1), 160°C (Zone 2), and 150°C (die). The masterbatch was first prepared by compounding 60:40 of HDPE-g-MA: modified Mt at a screw speed of 60 rpm. In a second extrusion, the dilution of the masterbatch by PLA at a screw speed of 130 rpm provided nanocomposites with modified Mt loadings of 5 and 8 php (named PLA/Ag-Mt-5, PLA/Ag-Mt-8, PLA/BDAC-Mt-5, PLA/BDAC-Mt-8, PLA/Ag20/BDAC80-Mt-5, and PLA/Ag20/BDAC80-Mt-8). The extrudates were then palletised and dried. The sheets were prepared by hot-pressing the nanocomposite pellets at 170°C and 450 kg/cm^2 for 5 min.

Structural and morphological analysis

Infrared spectra were recorded over the range of 400 - 4000 cm^{-1} with an Equinox 55 FTIR spectrometer (Bruker, Germany), using the conventional KBr pellet method with a nominal resolution of 4 cm^{-1}. For the KBr pelleting sample preparation, 1 mg of Mt powder was ground with 99 mg of KBr in an agate mortar and pestle. The mixture was then pressed into a disk using a hydraulic press.

Wide angle X-ray diffraction (WAXD) patterns were examined with an X'Pert MPD diffractometer (Philips, the Netherlands) with an incident wavelength (l) of 0.154 nm of CuKα radiation. The Mt powder was analysed in a 2q range of 1° to 10° and 30° to 80°, with a scanning rate of 1.0°/min, while the PLA and its nanocomposites were analysed in a 2θ range of 1° to 10°.

The morphology of the PLA/Ag20/BDAC80-Mt-5 nanocomposite was characterised by transmission electron microscopy (TEM; JEM-2010, JEOL, Japan). Ultrathin nanocomposite sections (70 - 100 nm) were obtained by cryogenic cutting with an ultramicrotome (Leica Ultracut UCT) equipped with a diamond knife. The sections were transferred to carbon-coated copper grids (200-mesh, with a Lacey support film).

Antifungal activity evaluation

Inoculation was performed by transferring mycelial plugs of 3-d-old colonies growing on a PDA medium with 5% (w/v) modified Mt samples. Antifungal activity was evaluated 1 d after inoculation, and everyday thereafter by measuring the colony diameters. All test plates were incubated at 37°C for 3 d for *F. moniliforme*, and 7 d for *P. roqueforti*. The experiments were performed in triplicate. The inhibition rate was calculated using Eq. 1 (Lamsal *et al*., 2011):

$$Inhibition\ rate\ (\%) = \frac{R-r}{R} \times 100 \qquad \text{(Eq. 1)}$$

where, R = radial growth of fungi on the PDA plate (control plate), and r = radial growth of fungi on the PDA plate containing the modified Mt sample.

In addition, spore germination on the nanocomposite film was assessed using an optical microscope (Eclipse 80i, Nikon, Japan). A volume of 20 µL of a spore suspension with an approximate concentration of 10^5 spores/mL was dropped onto the centre of the film sample, and incubated at ambient temperature for 15, 30, and 45 h (de Fátima Dias Diniz *et al*., 2022).

Tensile properties

The mechanical properties of PLA and its nanocomposites were evaluated by stress-strain measurements at room temperature, using a universal tensile testing machine (LR 30 K, Lloyd Instruments, UK) following the ASTM D638 protocol. The dumbbell-shaped test specimens had an overall length, width, and gauge length of 63.5, 3.18, and 7.60 mm, respectively. Young's modulus, tensile strength, and elongation at break were obtained from the measurements at a crosshead speed of 5 mm/min. Five specimens of each sample were used for the measurements.

Impact testing

Izod impact tests were performed on the notched impact specimens following the ASTM D256 protocol, using an impact tester (Zwick 5102.202, FR, Germany) under ambient conditions. Rectangular specimens, with a thickness of 2 mm, width of 15 mm, and length of 75 mm were prepared, and all specimens were notched at a 45° angle with a depth of 2 mm. Five specimens of each formulation were tested and the average values were reported.

Water vapour permeability (WVP)

WVP was measured following a modified ASTM method. An aluminium permeation cup was filled with dried silica gel (0% RH), and sealed with nanocomposite film, using silicone vacuum grease. The cup was then placed in a desiccator containing distilled water, and stored at 30°C. The weight gain of the cup was determined every 6 h for 48 h. The WVP of the film was calculated using Eq. 2:

$$WVP\ (\mathrm{g}\ m/m^2\mathrm{s\ Pa}) = (WVTR \times L)/\Delta\mathrm{p} \qquad \text{(Eq. 2)}$$

where, $WVTR$ = measured water vapour transmission rate (g $/m^2 s$) through the film, L = mean thickness (m), and Δp = partial water vapour pressure difference (Pa) across the film. Three replicates were used for the WVP testing.

Differential scanning calorimetry (DSC)

DSC analysis was carried out using a DSC-7 differential scanning calorimeter (Perkin Elmer, USA) to determine the thermal properties of PLA and its nanocomposites. Nitrogen was used as the carrier gas at a constant flow of 20 mL/min. The sample (5 – 10 mg) was sealed in an aluminium DSC pan, heated from room temperature to 180°C at a heating rate of 10°C/min, and held at 180°C for 3 min to eliminate the thermal history. The sample was then cooled to 25°C at a cooling rate of 10°C/min. A second heating scan from 25 to 180°C at 10°C/min was then performed to characterise the glass transition temperature (T_g), cold crystallisation temperature (T_{cc}), melting temperature (T_m), and specific fusion enthalpy (ΔH_m) of the sample. The degree of crystallinity (X_c) was calculated using Eq. 3:

$$X_c(\%) = \frac{\Delta H_m - \Delta H_{cc}}{\Delta H_m^0 \times w} \times 100 \qquad \text{(Eq. 3)}$$

where, ΔH_m = melting enthalpy (J/g), ΔH_{cc} = cold crystallisation enthalpy (J/g), ΔH_m^0 = theoretical melting enthalpy of the full crystallisation of PLA (93.7 J/g) (Gomez-Gamez *et al*., 2020), and w = weight fraction of PLA.

Overall migration test

The gravimetric overall migration analysis was conducted following the EU Regulation No 10/2011 protocol. The PLA/Ag20/BDAC80-Mt-5 sample (surface area of 1 dm^2) was completely immersed in 200 mL of selected food simulants, namely distilled water, ethanol (10%, v/v), and acetic acid (3%, w/v). Distilled water, ethanol, and acetic acid were chosen to represent foods that have a hydrophilic character, and can extract hydrophilic substances with pHs above 4.5, below 4.5, or in an alcoholic matrix (≥ 10% alcohol), respectively. The extractions were conducted at 70°C for 2 h for the intended food contact conditions (*i.e*., heating up to 70°C for up to 2 h, or up to 100°C for up to 15 min, not followed by long-term room or refrigerated temperature storage). Subsequently, a known aliquot of the extracted simulant was evaporated to dryness and the non-volatile solid residue was gravimetrically analysed. The overall migration values were calculated and expressed in mg/dm^2 of simulant. The tests were conducted in triplicate.

Statistical analysis

The analysed data were presented as mean ± standard deviation. The significance of the differences between the data was determined using a One-way analysis of variance (ANOVA). The values of the significant difference and mean were obtained by performing Duncan's test at a confidence level of $p < 0.05$.

Results and discussion

Fourier-transform infrared spectroscopy (FTIR)

The FTIR spectra of Ag/BDAC-Mt, Na^+-Mt, Ag-Mt, and BDAC-Mt are displayed in Figure 1. The characteristic bands of Na^+-Mt appeared at 3625 and 3437 cm^{-1} (assigned to the O-H stretching vibration), 1637 cm^{-1} (assigned to the O-H bending vibration), 1028 cm^{-1} (assigned to the Si-O stretching vibration), 839, 613, and 534 cm^{-1} (assigned to the Si-O and Al-O bending vibration) (Ohashi *et al*., 2009). The absorption due to Al-O-Si bending, where Al is an octahedral cation, was observed at 519 cm^{-1}; the Si-O-Si bending, at 445 cm^{-1}; and the Al-Al-OH

bending, at 914 cm^{-1}. This confirmed the presence of Mt. The aliphatic absorption bands, corresponding to methylene groups, appeared between 3000 and 2800 cm^{-1}, and between 1520 and 1400 cm^{-1} (Vaia *et al*., 1994). The asymmetric and symmetric stretching vibration bands of the -CH_2 group were observed at ~2920 and 2850 cm^{-1}, respectively. The bending of the C-H group for mono-substituted benzene appeared at 650 - 800 cm^{-1}. These bands were present in the BDAC-Mt and Ag/BDAC-Mt samples, but were not observed in Na^+-Mt or Ag-Mt. This finding revealed the successful intercalation of BDAC on Mt. Moreover, the out-of-plane stretching vibration band of the Si-O bonds within the tetrahedral silica layer in Na^+-Mt at ~1028 cm^{-1} shifted to a higher wavenumber around 1030 - 1034 cm^{-1} in modified Mt, confirming the intercalation on the Mt layers (Sarier *et al*., 2010). These results confirmed the successful deposition of silver and BDAC onto the Mt layers. In addition, silver nanoparticles were detected in the morphological study using TEM. Nonetheless, the vibration band of NO_3 (1350 - 1400 cm^{-1}) was not observed, indicating that no sizeable amount of free alkyl ammonium salt was entrapped in Ag/BDAC-Mt after washing with deionised water (Valaskova *et al*., 2010).

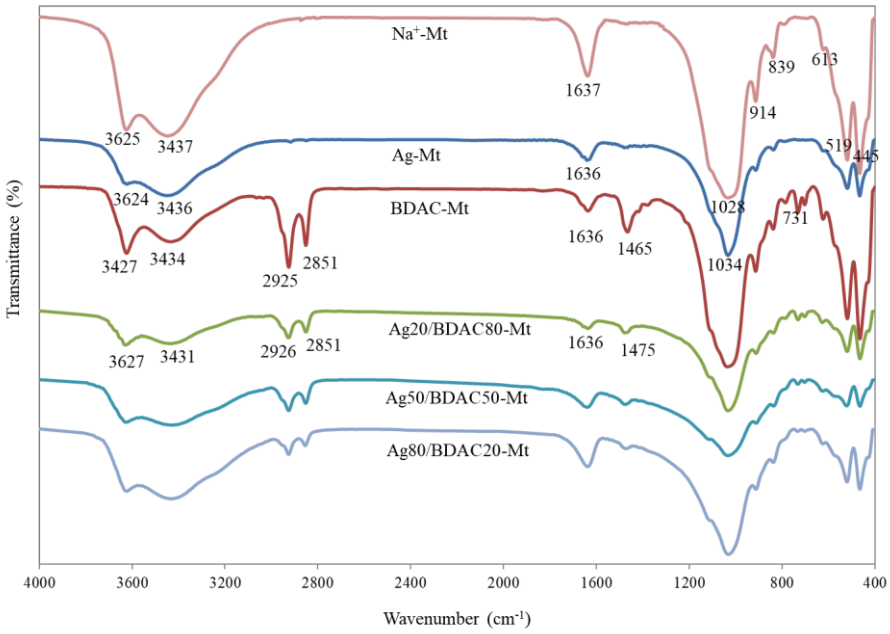

Figure 1. FTIR spectra of Ag/BDAC-Mt at different molar ratios, compared with Na^+-Mt, Ag-Mt, and BDAC-Mt.

Wide angle X-ray diffraction (WAXD)

The 2θ and calculated d-values of Na^+-Mt, Ag-Mt, BDAC-Mt, and Ag/BDAC-Mt are presented in Figure 2a and Table 1, respectively. The interaction of silver and BDAC with Na^+-Mt shifted the $d_{(001)}$ diffraction peak of Na^+-Mt toward lower 2θ values, implying an expansion of the interlayer space. The d-values of Na^+-Mt increased from 1.25 to 1.49 nm for Ag-Mt, and to 1.83, 1.75, 1.56, and 1.51 nm for BDAC-Mt, Ag20/BDAC80-Mt, Ag50/BDAC50-Mt, and Ag80/BDAC20-Mt, respectively. This indicated that the d-value of Mt depends on the surfactant loading. The d-value increased with an increasing BDAC amount; thus, BDAC-Mt showed the highest d-value, indicating the greatest intercalation. Ag/BDAC-Mt at all Ag and BDAC ratios showed higher d-values than those of Ag-Mt and Na^+-Mt, suggesting dispersion improvement.

The WAXD patterns in the range of $35^o < 2\theta < 80^o$ revealed the crystalline structure of the silver nanoparticles in Mt. Ag/BDAC-Mt at different molar ratio percentages, compared with Na^+-Mt (Figure 2b). The reflections at $2\theta = 38.3^o$, 46.2^o, 64.5^o, and 77.3^o were attributed to the 111, 200, 220, and 331 crystallographic planes of the silver crystals (Benhacine *et al*., 2016; Fernández Solarte *et al*., 2019). Moreover, the characteristic reflection at $2\theta = 54.4^o$ and 62.1^o was associated with the Na^+-Mt (Sarier *et al*., 2010; Shameli *et al*., 2011). These results confirmed the presence of silver in the Ag/BDAC-Mt samples.

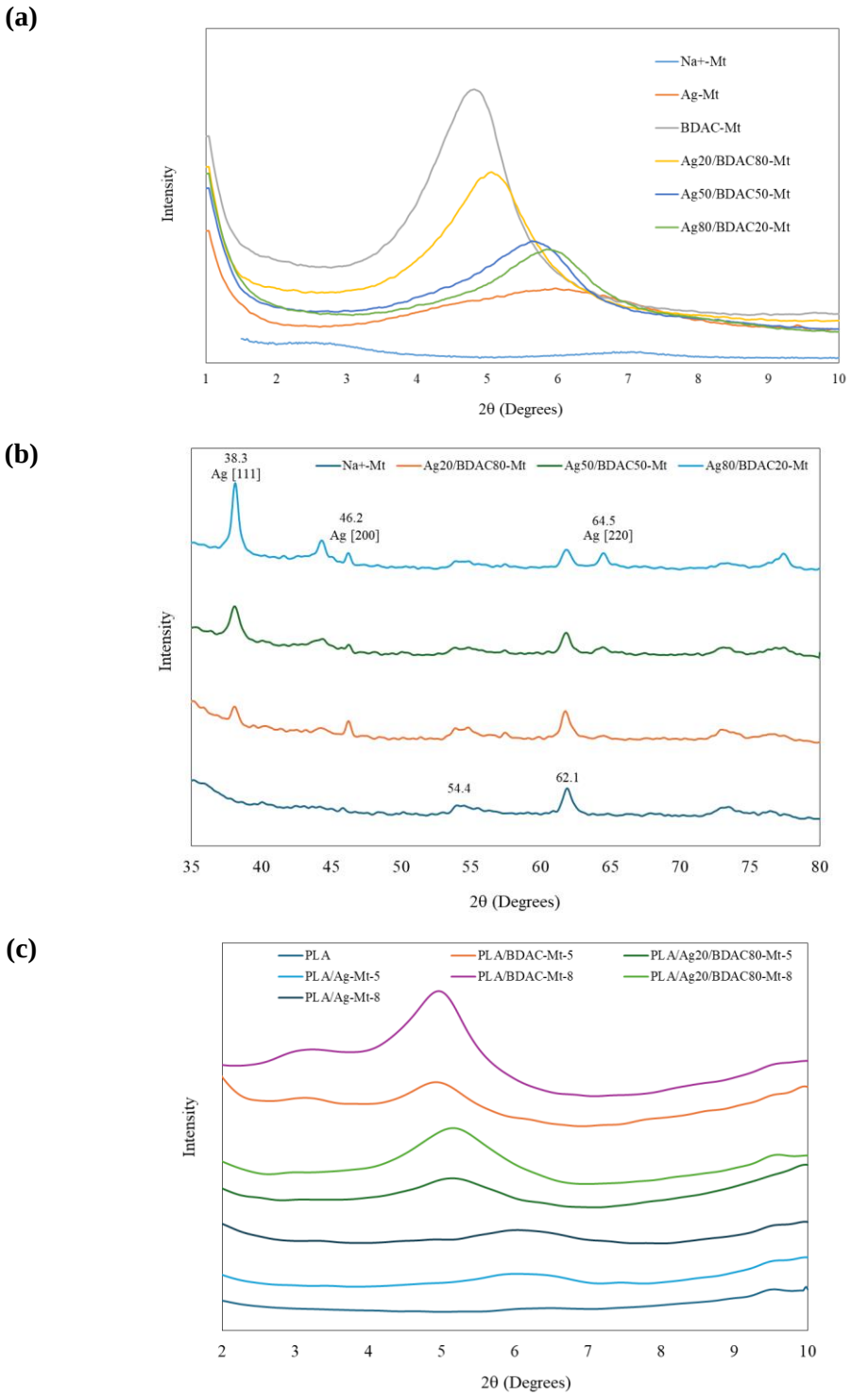

Figure 2. (a) WAXD patterns (2θ = 1° - 10°), and **(b)** WAXD patterns (2θ = 35° - 80°) of Ag/BDAC-Mt at different molar ratios, compared with Na^+-Mt **(c)** WAXD pattern of neat PLA and its nanocomposites.

Table 1. Values of 2θ and d_{001} for Na^+-Mt, Ag-Mt, BDAC-Mt, Ag/BDAC-Mt, and nanocomposites at 5 and 8 php of modified-Mt.

Sample	2θ (degrees)	d_{001} (nm)
Na^+-Mt	7.04	1.25
Ag-Mt	5.92	1.49
BDAC-Mt	4.82	1.83
Ag20/BDAC80-Mt	5.04	1.75
Ag50/BDAC50-Mt	5.66	1.56
Ag80/BDAC20-Mt	5.84	1.51
PLA/Ag-Mt-5	5.88	1.50
PLA/Ag20/BDAC80-Mt-5	4.98	1.77
PLA/BDAC-Mt-5	4.76	1.85
PLA/Ag-Mt-8	5.96	1.48
PLA/Ag20/BDAC80-Mt-8	5.23	1.69
PLA/BDAC-Mt-8	4.93	1.79

WAXD analysis (Figure 2c) of PLA and its nanocomposites revealed that the differences in the interlayer spacing were related to the type of intercalation agent that penetrated between the clay layers. The highest d-spacing corresponded to PLA/BDAC-Mt, followed by PLA/Ag20/BDAC80-Mt and PLA/Ag-Mt (Table 1). These results indicated that the intercalating agents and PLA chains entered the Na^+- Mt. The d-spacing of PLA/Ag-Mt was close to that of Na^+-Mt (1.49 - 1.50 nm).

Transmission electron microscopy (TEM)

The PLA/Ag20/BDAC80-Mt-5 nano composites were subjected to TEM analysis to support the WAXD results by visualising the dispersion of the clay and silver particles in the polymer matrix. Figure 3 displays the TEM images. The dark grey lines and dark particles correspond to the Mt layers and silver particles, respectively, in the PLA matrix (bright areas). The TEM images revealed that the Mt layers in the PLA matrix were randomly distributed, and a partially intercalating structure was observed. However, some areas in the images exhibited agglomeration or clay tactoids, indicating incomplete intercalation because of the filler-filler interaction of Mt. In addition, silver particles were deposited on the Mt surface, suggesting they were also deposited on the Mt layers.

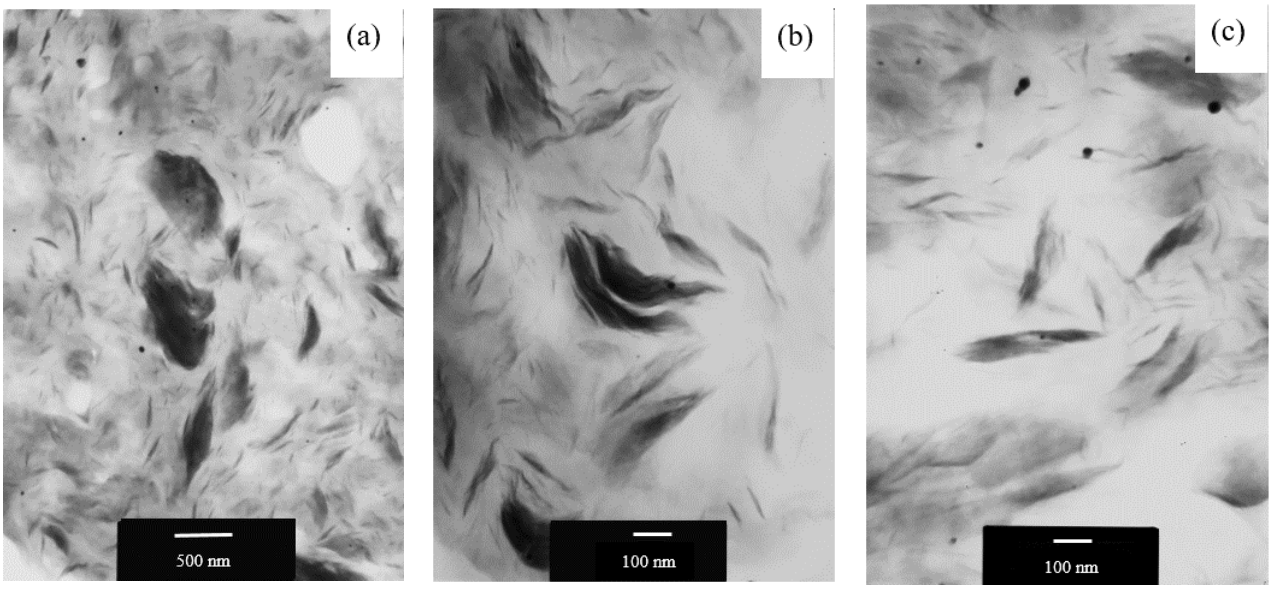

Figure 3. TEM images of PLA/Ag20/BDAC80-Mt-5 nanocomposites: **(a)** at 15,000× magnification, and **(b)** and **(c)** at 50,000× magnification.

Antifungal activity

The radial growth and inhibitory rate of modified Mt were evaluated and compared with those of the control (PDA media) (Figures 4a and 4b, respectively). Ag-Mt completely inhibited the growth of both *P. roqueforti* and *F. moniliforme*. The mycelium growth inhibition rate (Figure 4c) of BDAC-Mt was 89% for *P. roqueforti*, and 32% for *F. moniliforme* after 7 and 3 d of inoculation, respectively. This suggested that different fungal strains may display differences in sensitivity, even for the same sample under identical growth conditions. Moreover, Ag/BDAC-Mt showed less mycelial growth inhibition for both fungi than Ag-Mt and its

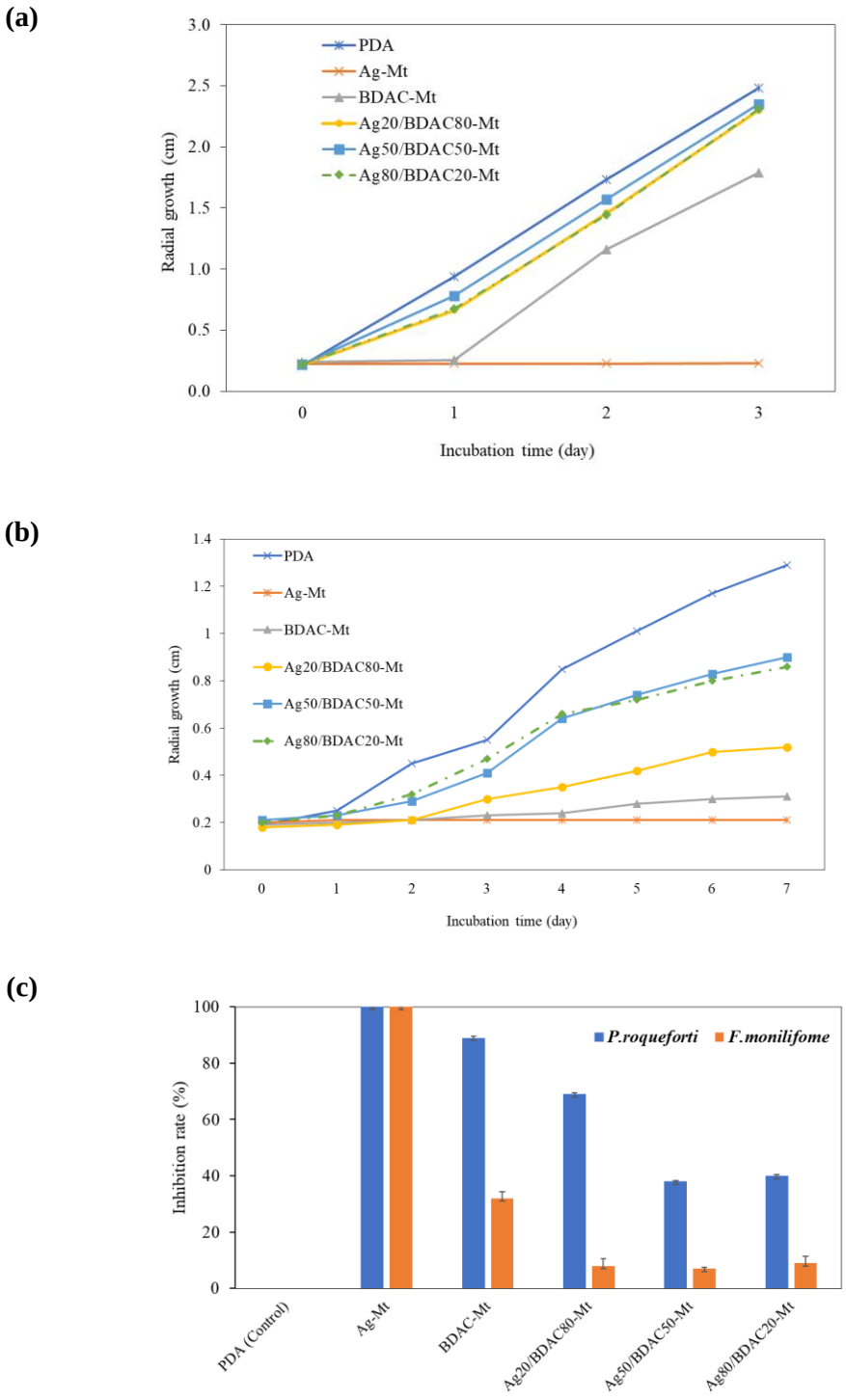

Figure 4. Radial growth of **(a)** *F. moniliforme* and **(b)** *P. roqueforti* inoculated on Ag-Mt, BDAC-Mt, Ag20/BDAC80, Ag50/BDAC50-Mt, and Ag80/BDAC20-Mt, compared to control (PDA), and **(c)** inhibitory rate (%) of Ag-Mt, BDAC-Mt, and Ag/BDAC-Mt against *P. roqueforti* and *F. moniliforme*.

BDAC-Mt counterparts ($p < 0.05$). For *F. moniliforme*, no differences were observed for Ag/BDAC-Mt of all compositions. For *P. roqueforti*, higher silver amounts resulted in less inhibition, and low activity was observed for Ag50/BDAC50-Mt and Ag80/BDAC20-Mt. These data suggested that the amount of BDAC and chain arrangement—which causes silver aggregation—may reduce the antifungal activity of the films. A previous study evaluated the inhibitory action of silver against fungi, and reported that it inhibited the protein expression associated with ATP production, and disrupted membrane integrity, leading to failed ribosome synthesis and DNA replication, and finally, cell apoptosis (Roy *et al*., 2020). Moreover, the antifungal activity of BDAC was enhanced by the absorption and penetration of BDAC into the cell wall, altering the permeability of cytoplasmic membranes, and causing intracellular substances to extravasate and degrade (Zhao *et al*., 2024).

The antifungal activities of the PLA/Ag-Mt, PLA/Ag20/BDAC80-Mt, and PLA/Ag-Mt nano composites were qualitatively evaluated against *P. roqueforti*, and spore germination was monitored by optical microscopy at 15, 30, and 45 h. Figure 5a shows that neat PLA did not exhibit antifungal activity, whereas PLA/Ag-Mt completely inhibited spore germination (Figures 5f and 5g). Spores on the PLA sample germinated at 15 h, and continued to grow rapidly thereafter. For PLA/BDAC-Mt, spore germination and mycelial growth occurred after approximately 30 h. The PLA/Ag20/BDAC80-Mt-8 nanocomposite had a greater inhibitory effect on spore germination and fungal growth than PLA/Ag20/BDAC80-Mt-5 (Figures 5d and 5e).

Mechanical properties

Tensile and impact tests were performed to investigate the influence of modified Mt (at 5 and 8 php) on the mechanical properties of PLA-based nanocomposites. The results are shown in Table 2. Compared to neat PLA, the tensile strength and elongation at break of the PLA nanocomposites decreased by 20 - 40% and 20 - 34%, respectively, depending on the type of modified Mt and loading. This trend agreed with previous reports, and was probably due to the attraction between the clay and the polymer matrix being disturbed by the clay tactoids. Incorporating a high amount of modified Mt resulted in poor dispersion in the PLA matrix, leading to agglomeration and phase separation (Rhim *et al*., 2009; Balakrishnan *et al*., 2010). Although the tensile strength of the nanocomposites decreased, it was still comparable to that of widely used plastics such as polypropylene (PP, 31 - 38 MPa) and polystyrene (PS, 45 - 83 MPa). The decrease in chain mobility reduced the elongation at break of the nanocomposites, which agreed with previous reports (Bezerra Lima *et al*., 2021).

However, Young's moduli of the PLA nanocomposites increased by 13 - 27%, with PLA/Ag20/BDAC80-Mt-5 exhibiting the greatest improvement. This suggested that the high aspect ratio and surface area of nanoclay in the PLA matrix as well as using HDPE-g-MA as a compatibiliser transfer the stress to the clay layers (Balakrishnan *et al*., 2010).

WVP

The WVP of the nanocomposite films at 5 php of modified Mt varied significantly ($p < 0.05$) depending on the type of modified Mt used (Table 3). The WVP of nanocomposite films incorporated with Ag-Mt decreased slightly, while that of PLA films compounded with BDAC-Mt or Ag20/BDAC80-Mt increased slightly compared to neat PLA. This result suggested that Ag-Mt was dispersed in the PLA matrix, and formed a tortuous path for water vapour diffusion, increasing the effective diffusion path length (Rhim *et al*., 2009).

DSC

DSC was performed to investigate the thermal transition of PLA and its nanocomposites, and the results are presented in Table 3. The analysis of the second heating showed that neat PLA had a T_g of approximately 59°C, T_{cc} of 124°C, and T_{m2} of 150°C. PLA and its nanocomposites did not exhibit a crystallisation temperature during cooling. This behaviour has also been reported for PLA/LDPE/OC nanocomposites, and could be explained by the slow crystallisation rate of PLA during cooling (Balakrishnan *et al*., 2010). The T_g and T_{cc} of all PLA nanocomposites significantly decreased compared with that of the neat PLA, regardless of the type of modified Mt used. The decrease in T_g might have been due to the addition of HDPE-g-MA, and might be associated with the plasticising effect of HDPE-g-

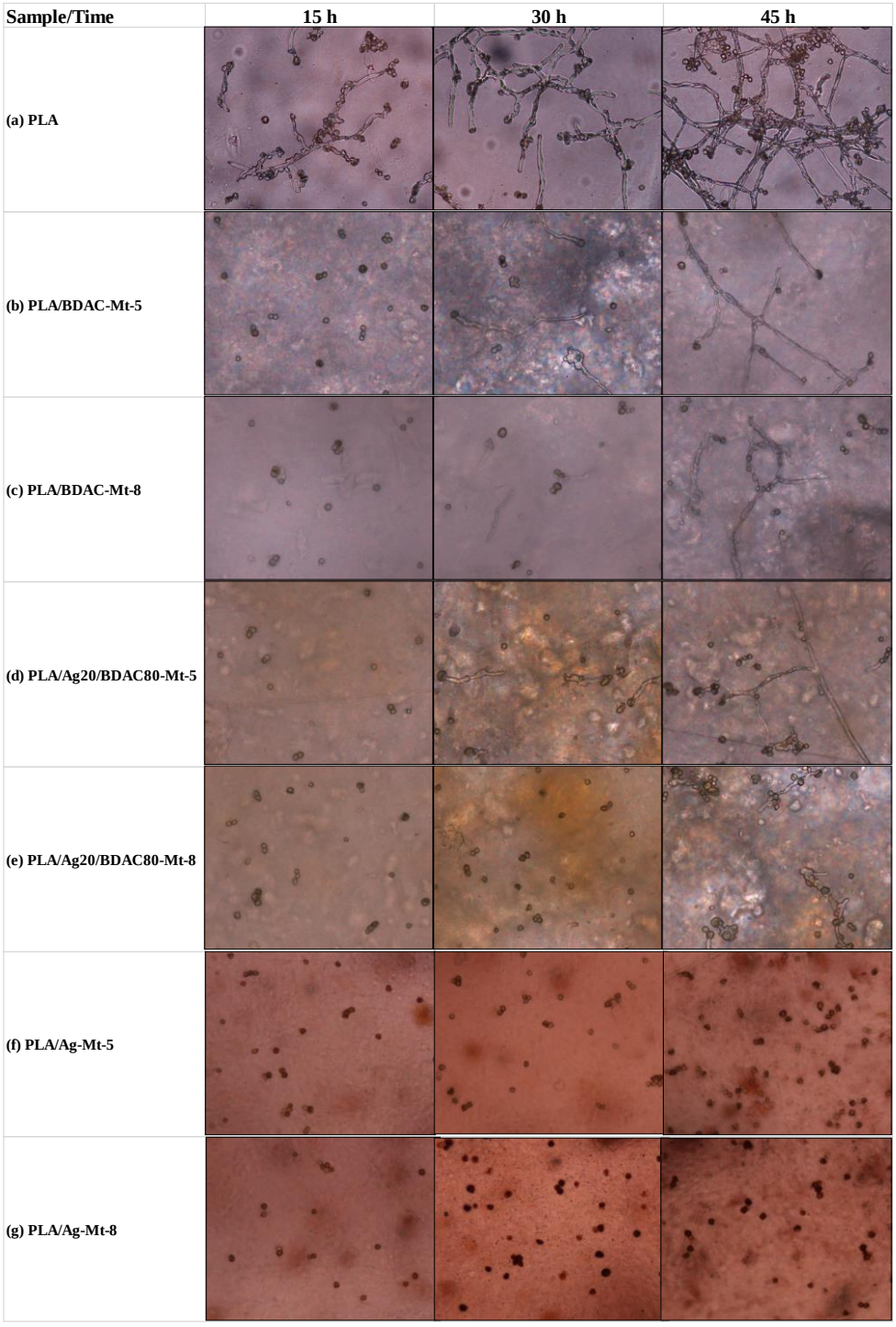

Figure 5. Microscopy photograph of *P. roqueforti* spores on neat PLA and its PLA nanocomposites at 15, 30, and 45 h.

Table 2. Mechanical properties of neat PLA and its nanocomposites.

Sample	Young's modulus (GPa)	Tensile strength (MPa)	Elongation at break (%)	Impact strength (J/m)
PLA	2.44 ± 0.10^{d}	54.56 ± 1.20^{a}	3.35 ± 0.02^{a}	25.29 ± 1.31^{b}
PLA/BDAC-Mt-5	3.10 ± 0.16^{a}	42.37 ± 1.34^{b}	2.55 ± 0.12^{b}	26.58 ± 1.96^{b}
PLA/BDAC-Mt-8	2.97 ± 0.22^{ab}	33.48 ± 1.65^{e}	2.22 ± 0.18^{d}	21.83 ± 0.66^{c}
PLA/Ag20/BDAC80-Mt-5	2.95 ± 0.16^{ab}	43.58 ± 1.21^{b}	2.68 ± 0.08^{b}	30.42 ± 1.11^{a}
PLA/Ag20/BDAC80-Mt-8	2.88 ± 0.10^{b}	35.57 ± 1.27^{d}	2.37 ± 0.08^{c}	26.48 ± 1.56^{b}
PLA/Ag-Mt-5	2.65 ± 0.09^{c}	39.97 ± 1.52^{c}	2.64 ± 0.11^{b}	25.75 ± 1.26^{b}
PLA/Ag-Mt-8	2.53 ± 0.12^{cd}	32.54 ± 1.77^{e}	2.26 ± 0.13^{cd}	20.43 ± 1.28^{d}

All values are mean ± standard deviation of five replicates (n = 5). Means followed by different lowercase superscripts in the same column are significantly different ($p < 0.05$).

Table 3. Values of WVP and DSC for PLA and its nanocomposites.

Sample	WVP	DSC					
	(10^{-11} g m/m^2 s Pa)	T_g (°C)	T_{cc} (°C)	T_{m1} (°C)	T_{m2} (°C)	ΔH_m (J/g)	X_c (%)
PLA	2.01 ± 0.12^{ab}	59.26	124.33	-	150.66	2.27	2.42
PLA/BDAC-Mt-5	2.62 ± 0.30^{bc}	57.63	115.63	126.17	149.50	23.01	24.60
PLA/Ag-Mt-5	1.71 ± 0.10^{ab}	57.93	115.50	126.50	150.83	23.10	24.70
PLA/Ag20/BDAC80-Mt-5	2.37 ± 0.27^{bc}	57.66	116.33	125.83	149.33	23.10	24.70

All values are mean ± standard deviation of three replicates (n = 3). Means followed by different lowercase superscripts in the same column are significantly different ($p < 0.05$).

MA according to a previous report that described a PE-g-MA-compatibilised PE/halloysite nanotube nanocomposite (Sikora *et al*., 2019). The decrease in T_{cc} was attributed to the nanoclay in the PLA matrix, which acted as an effective nucleating agent for polymer crystallisation, enhancing crystallinity (Balakrishnan *et al*., 2010). The endothermic melting peaks at approximately 126 and 150°C represent the melting temperatures of HDPE-g-MA and PLA, respectively. Incorporating nanoclay did not affect the melting temperatures of the PLA nanocomposites, which agreed with the findings of other researchers (Shyang and Kuen, 2008; Balakrishnan *et al*., 2010).

Overall migration

To comply with food contact material legislation according to the most recent EU legislation (Reg. EU 10/2011 and amendments), the total mass of non-volatile migrants released into the selected food simulants was determined. For the PLA/Ag20/BDAC80-Mt-5 nanocomposite, the overall migration values were 1.7 ± 0.2, 2.5 ± 0.2, and 0.9 ± 0.1 mg/dm^2 in distilled water, 10% (v/v) ethanol, and 3% (w/v) acetic acid, respectively. The highest value was observed in 10% ethanol, and can be attributed to the potential hydrolytic degradation of the PLA chain, involving swelling, plasticisation, and crystallisation (Iñiguez-Franco *et al*., 2016). This finding was also consistent with a study that suggested that ethanol may cause the stepwise degradation of PLA (Yanat *et al*., 2023). However, the overall migration values in all three simulants were well below the regulatory limit of 10 mg/dm^2 (60 mg/kg food) set by the current EU legislation (Scarfato *et al*., 2017). This suggested that PLA/Ag20/BDAC80-Mt-5 is safe for use in food packaging. Nevertheless, further assessments, such as specific migration tests and toxicological evaluations, should be conducted to establish the safety of this material for future food packaging applications.

Conclusion

Silver/benzyl dodecyl dimethylammonium chloride-modified montmorillonite (Ag/BDAC-Mt) was prepared *via* a simple intercalation reaction using different proportions of silver nitrate and BDAC cationic surfactant. The montmorillonite modified with a ratio of 20:80 of Ag:BDAC (Ag20/BDAC80-Mt) was selected to prepare the PLA-based nanocomposites at 5 and 8 php. The properties of the nanocomposites were characterised. PLA/Ag20/BDAC80-Mt-5 exhibited the highest impact strength. Compared with neat PLA, the tensile

strength and elongation at break of the nanocomposites decreased depending on the type of modified Mt and their added amount. The water vapour permeability (WVP) was comparable to that of neat PLA. The antifungal activity of Ag-Mt, BDAC-Mt, and Ag/BDAC-Mt against foodborne pathogenic and mycotoxigenic strains (*F. moniliforme* and *P. roqueforti*) was demonstrated. However, the nanocomposites showed inhibition against only *P. roqueforti*. The present work thus demonstrated the potential of Ag/BDAC-Mt as a new antifungal agent that also helps enhance the impact strength of PLA nanocomposites with potential food packaging applications.

Acknowledgement

The authors express their sincere thanks to the Prince of Songkla University, Hat Yai, Songkhla, Thailand for the financial support received for the completion of the present work (grant no.: AGR540667S).

References

Auras, R., Harte, B. and Selke, S. 2004. An overview of polylactides as packaging materials. Macromolecular Bioscience 4: 835-864.

Balakrishnan, H., Hassan, A., Wahit, M. U., Yussuf, A. A. and Razak, S. B. A. 2010. Novel toughened polylactic acid nanocomposite: Mechanical, thermal and morphological properties. Materials and Design 31: 3289-3298.

Benhacine, F., Hadj-Hamou, A. and Habi, A. 2016. Development of long-term antimicrobial poly (ε-caprolactone)/silver exchanged montmorillonite nanocomposite films with silver ion release property for active packaging use. Polymer Bulletin 73: 1207-1227.

Bezerra Lima, E. M., Middea, A., Marconcini, J. M., Corrêa, A. C., Fernandes Pereira, J., Vieira Guimarães, A., … and Neumann, R. 2021. Biodegradable PLA based nanocomposites for packaging applications: The effects of organo-modified bentonite concentration. Journal of Applied Polymer Science 138.

de Fátima Dias Diniz, G., Cota, L. V., Figueiredo, J. E. F., Aguiar, F. M., da Silva, D. D., de Paula Lana, U. G., … and de Oliveira-Paiva, C. A. 2022. Antifungal activity of bacterial strains from maize silks against *Fusarium verticillioides*. Archives of Microbiology 204: 89.

Dharini, V., Periyar Selvam, S., Jayaramudu, J. and Sadiku Emmanuel, R. 2022. Functional properties of clay nanofillers used in the biopolymer-based composite films for active food packaging applications - Review. Applied Clay Science 226: 106555.

Fernández Solarte, A. M., Villarroel-Rocha, J., Morantes, C. F., Montes, M. L., Sapag, K., Curutchet, G. and Torres Sánchez, R. M. 2019. Insight into surface and structural changes of montmorillonite and organomontmorillonites loaded with Ag. Comptes Rendus Chimie 22: 142-153.

Gomez-Gamez, A. B., Yebra-Rodriguez, A., Peñas-Sanjuan, A., Soriano-Cuadrado, B. and Jimenez-Millan, J. 2020. Influence of clay percentage on the technical properties of montmorillonite/polylactic acid nanocomposites. Applied Clay Science 198: 105818.

Haubert, L., Zehetmeyr, M. L., Pereira, Y. M. N., Kroning, I. S., Maia, D. S. V., Sehn, C. P., … and da Silva, W. P. 2019. Tolerance to benzalkonium chloride and antimicrobial activity of *Butia odorata* Barb. Rodr. extract in *Salmonella* spp. isolates from food and food environments. Food Research International 116: 652-659.

Hong, S. I., Wang, L. F. and Rhim, J. W. 2022. Preparation and characterization of nanoclays-incorporated polyethylene/ thermoplastic starch composite films with antimicrobial activity. Food Packaging and Shelf Life 31: 100784.

Iñiguez-Franco, F., Auras, R., Burgess, G., Holmes, D., Fang, X., Rubino, M. and Soto-Valdez, H. 2016. Concurrent solvent induced crystallization and hydrolytic degradation of PLA by water-ethanol solutions. Polymer 99: 315-323.

Kant, P., Reinprecht, Y., Martin, C. J., Islam, R. and Pauls, K. P. 2017. 4.65 - Disease resistance. In Moo-Young, M. (ed). Comprehensive Biotechnology, 3rd ed, p. 789-805. United States: Elsevier.

Khalil, R. K. S. 2013. Selective removal and inactivation of bacteria by nanoparticle composites prepared by surface modification

of montmorillonite with quaternary ammonium compounds. World Journal of Microbiology and Biotechnology 29: 1839-1850.

Lamsal, K., Kim, S. W., Jung, J. H., Kim, Y. S., Kim, K. S. and Lee, Y. S. 2011. Application of silver nanoparticles for the control of *Colletotrichum* species *in vitro* and pepper anthracnose disease in field. Mycobiology 39: 194-199.

Moeini, A., Germann, N., Malinconico, M. and Santagata, G. 2021. Formulation of secondary compounds as additives of biopolymer-based food packaging: A review. Trends in Food Science and Technology 114: 342-354.

Moeini, A., Mallardo, S., Cimmino, A., Dal Poggetto, G., Masi, M., Di Biase, M., … and Santagata, G. 2020. Thermoplastic starch and bioactive chitosan sub-microparticle biocomposites: Antifungal and chemico-physical properties of the films. Carbohydrate Polymers 230: 115627.

Mohapatra, S., Yutao, L., Goh, S. G., Ng, C., Luhua, Y., Tran, N. H. and Gin, K. Y. H. 2023. Quaternary ammonium compounds of emerging concern: Classification, occurrence, fate, toxicity and antimicrobial resistance. Journal of Hazardous Materials 445: 130393.

Moustafa, H., El-Sayed, S. M. and Youssef, A. M. 2023. Synergistic impact of cumin essential oil on enhancing of UV-blocking and antibacterial activity of biodegradable poly(butylene adipate-co-terephthalate)/clay platelets nanocomposites. Journal of Thermoplastic Composite Materials 36: 96-117.

Ohashi, F., Ueda, S., Taguri, T., Kawachi, S. and Abe, H. 2009. Antimicrobial activity and thermostability of silver 6-benzylaminopurine montmorillonite. Applied Clay Science 46: 296-299.

Priyadarshi, R., Roy, S., Ghosh, T., Biswas, D. and Rhim, J. W. 2022. Antimicrobial nanofillers reinforced biopolymer composite films for active food packaging applications - A review. Sustainable Materials and Technologies 32: e00353.

Rhim, J. W., Hong, S. I. and Ha, C. S. 2009. Tensile, water vapor barrier and antimicrobial properties of PLA/nanoclay composite films. LWT – Food Science and Technology 42: 612-617.

Roy, A., Joshi, M., Butola, B. S. and Ghosh, S. 2020. Evaluation of biological and cytocompatible properties in nano silver-clay based polyethylene nanocomposites. Journal of Hazardous Materials 384: 121309.

Santagata, G., Valerio, F., Cimmino, A., Dal Poggetto, G., Masi, M., Di Biase, M., ... and Evidente, A. 2017. Chemico-physical and antifungal properties of poly(butylene succinate)/cavoxin blend: Study of a novel bioactive polymeric based system. European Polymer Journal 94: 230-247.

Sarier, N., Onder, E. and Ersoy, S. 2010. The modification of Na-montmorillonite by salts of fatty acids: An easy intercalation process. Colloids and Surfaces A - Physicochemical and Engineering Aspects 371: 40-49.

Scarfato, P., Di Maio, L., Milana, M. R., Giamberardini, S., Denaro, M. and Incarnato, L. 2017. Performance properties, lactic acid specific migration and swelling by simulant of biodegradable poly(lactic acid)/nanoclay multilayer films for food packaging. Food Additives and Contaminants - Part A 34: 1730-1742.

Shameli, K., Ahmad, M. B., Zargar, M., Yunus, W. M., Rustaiyan, A. and Ibrahim, N. A. 2011. Synthesis of silver nanoparticles in montmorillonite and their antibacterial behavior. International Journal of Nanomedicine 6: 581-590.

Shi, J., Zhang, R., Liu, X., Zhang, Y., Du, Y., Dong, H., … and Chen, F. 2023. Advances in multifunctional biomass-derived nanocomposite films for active and sustainable food packaging. Carbohydrate Polymers 301: 120323.

Shyang, C. W. and Kuen, L. S. 2008. Flexural, morphological and thermal properties of poly(lactic acid)/ organo-montmorillonite nanocomposites. Polymers and Polymer Composites 16: 263 - 270.

Sikora, J. W., Gajdoš, I. and Puszka, A. 2019. Polyethylene-matrix composites with halloysite nanotubes with enhanced physical/thermal properties. Polymers 11: 787.

Tola, M. and Kebede, B. 2016. Occurrence, importance and control of mycotoxins: A review. Cogent Food and Agriculture 2: 1191103.

Vaia, R. A., Teukolsky, R. K. and Giannelis, E. P. 1994. Interlayer structure and molecular environment of alkylammonium layered silicates. Chemistry of Materials 6: 1017-1022.

Valaskova, M., Hundakova, M., Kutlakova, K. M., Seidlerova, J., Capkova, P., Pazdziora, E., … and Rafaja, D. 2010. Preparation and characterization of antibacterial silver/vermiculites and silver/montmorillonites. Geochimica et Cosmochimica Acta 74: 6287-6300.

Valerio, F., Masi, M., Cimmino, A., Moeini, S. A., Lavermicocca, P. and Evidente, A. 2018. Antimould microbial and plant metabolites with potential use in intelligent food packaging. Natural Product Research 32: 1605-1610.

Yanat, M., Muthurajan, M., Strubel, M., Grolle, K. and Schroën, K. 2023. Polylactic acid films reinforced with chitin nanocrystals: Biodegradation and migration behavior. Food Packaging and Shelf Life 40: 101217.

Zhang, L., Chen, J., Yu, W., Zhao, Q. and Liu, J. 2018. Antimicrobial nanocomposites prepared from montmorillonite/Ag^{+}/quaternary ammonium nitrate. Journal of Nanomaterials 2018: 190251.

Zhao, D., Zhang, Y., Jin, Z., Bai, R., Wang, J., Wu, L. and He, Y. 2024. Benzalkonium chloride and benzethonium chloride effectively reduce spore germination of ginger soft rot pathogens: *Fusarium solani* and *Fusarium oxysporum*. Journal of Fungi 10: 8.

Zhong, Y., Godwin, P., Jin, Y. and Xiao, H. 2020. Biodegradable polymers and green-based antimicrobial packaging materials: A mini-review. Advanced Industrial and Engineering Polymer Research 3: 27-35.